Biochimica et Biophysica Acta 1838 (2014) 3097–3106

Contents lists available at ScienceDirect

Biochimica et Biophysica Acta

journal homepage: www.elsevier.com/locate/bbamem

Multivalent presentation of the cell-penetrating peptide nona-arginine on a linear scaffold strongly increases its membrane-perturbing capacity ☆

Alokta Chakrabarti [a,1], J. Joris Witsenburg [a], Michael D. Sinzinger [a], Martin Richter [b], Rike Wallbrecher [a], Judith C. Cluitmans [a], Wouter P.R. Verdurmen [a,2], Sabine Tanis [a], Merel J.W. Adjobo-Hermans [a], Jörg Rademann [b,c], Roland Brock [a,*]

[a] Department of Biochemistry, Radboud Institute for Molecular Life Sciences, Radboud University Medical Centre, Geert Grooteplein 28, 6525 GA Nijmegen, the Netherlands
[b] Leibniz Institute for Molecular Pharmacology (FMP), Robert-Rössle-Str. 10, 13125 Berlin, Germany
[c] Medicinal Chemistry, Free University Berlin, Königin-Luise-Str. 2 + 4, 14195 Berlin, Germany

ARTICLE INFO

Article history:
Received 21 April 2014
Received in revised form 23 July 2014
Accepted 1 August 2014
Available online 7 August 2014

Keywords:
Cell-penetrating peptide
Drug delivery
Nona-arginine
Multivalency
Sphingomyelinase
Protein–protein interactions

ABSTRACT

Arginine-rich cell-penetrating peptides (CPP) are widely employed as delivery vehicles for a large variety of macromolecular cargos. As a mechanism-of-action for induction of uptake cross-linking of heparan sulfates and interaction with lipid head groups have been proposed. Here, we employed a multivalent display of the CPP nona-arginine (R9) on a linear dextran scaffold to assess the impact of heparan sulfate and lipid interactions on uptake and membrane perturbation. Increased avidity through multivalency should potentiate molecular phenomena that may only play a minor role if only individual peptides are used. To this point, the impact of multivalency has only been explored for dendrimers, CPP-decorated proteins and nanoparticles. We reasoned that multivalency on a linear scaffold would more faithfully mimic the arrangement of peptides at the membrane at high local peptide concentrations. On average, five R9 were coupled to a linear dextran backbone. The conjugate displayed a direct cytoplasmic uptake similar to free R9 at concentrations higher than 10 μM. However, this uptake was accompanied by an increased membrane disturbance and cellular toxicity that was independent of the presence of heparan sulfates. In contrast, for erythrocytes, the multivalent conjugate induced aggregation, however, showed only limited membrane perturbation. Overall, the results demonstrate that multivalency of R9 on a linear scaffold strongly increases the capacity to interact with the plasma membrane. However, the induction of membrane perturbation is a function of the cellular response to peptide binding.

1. Introduction

Conjugation to cell-penetrating peptides (CPPs) is considered a highly promising strategy to mediate cellular delivery of molecules that otherwise poorly enter cells [1–3]. Natural and synthetic CPPs are continuously being (re-)designed to improve delivery [4,5]. In contrast to the original concept of the CPP acting as a Trojan horse that passages passively through the plasma membrane by virtue of its structural characteristics it has become clear that with the exception of direct membrane permeation at low concentrations [6,7] CPPs actively induce cellular uptake [8]. In particular for large molecular weight cargos, endocytosis is the route of uptake [9]. Furthermore, at concentrations above about 10 μM, arginine-rich CPPs induce activation of acid sphingomyelinase, which leads to rapid cytoplasmic import via ceramide-rich membrane microdomains [10,11].

While the molecular mechanism underlying the activation of acid sphingomyelinase has not been resolved, for induction of endocytosis, it has been proposed that binding to negatively charged oligosaccharides of the glycocalyx leads to a clustering of syndecans [12], which activates Rac-dependent actin remodeling [13]. However, uptake is also observed for cells that are poor in glycosaminoglycans such as Jurkat T cell leukemia cells which calls for the involvement of additional processes [11].

Strikingly, in spite of its activity as a CPP, for nona-arginine (R9) little to no enrichment at cellular membranes is observed. Only when

Abbreviations: CPP, cell-penetrating peptide; R9, nona-arginine; Dex-$(R9)_5$, pentavalent display of R9 on a linear dextran backbone; PI, propidium iodide; N.A., numerical aperture; FBS, fetal bovine serum; PBS, phosphate-buffered saline; BSA, bovine serum albumin

☆ The authors declare no competing financial interests.

* Corresponding author at: Department of Biochemistry (286), Radboud Institute for Molecular Life Sciences, Radboud University Medical Centre, Geert Grooteplein 28, 6525 GA Nijmegen, the Netherlands. Tel.: +31 24 3666213; fax: +31 24 3616413.
E-mail address: r.brock@ncmls.ru.nl (R. Brock).
[1] Present address: Institute of Pharmaceutical Sciences, Albert-Ludwigs-Universität Freiburg, Albertstraße 25, 79104 Freiburg, Germany.
[2] Present address: Department of Biochemistry, University of Zurich, Winterthurerstrasse 190, 8057 Zurich, Switzerland.

http://dx.doi.org/10.1016/j.bbamem.2014.08.001
0005-2736/

internalization is compromised, a staining of the plasma membrane is visible which can be attributed to the interaction with glycosaminoglycans [14]. This indicates that in spite of a documented ability to interact with the head groups of the lipid bilayer and the capacity to partition into a hydrophobic environment in the presence of negatively charged chelating groups [15–17], on cells there is little enrichment at the level of the plasma membrane. Also, among a panel of nine tested CPPs R9 had the least membrane-disruptive potential [18], overall indicating that enrichment at the plasma membrane plays only a small role in the uptake of this CPP.

The geometry in which positive charge is presented greatly influences uptake efficiency. On one hand, it has been demonstrated that import can be enhanced through rigidifying the peptide backbone through cyclization [19]. On the other hand, multivalency is a well-established principle to potentiate molecular interactions through introduction of avidity [20–22]. Multivalent interactions in nature include binding of DNA at several sites by transcription factors, like the retinoid X receptor [20] or immunogenic recognition by multivalent antibodies such as IgM [23]. In the context of CPPs, oligoarginines are an example for a multivalent display of the guanidino-group and up to a certain length, activity of oligoarginines increases with the number of residues [24,25]. With respect to a multivalent display of CPPs, multivalency has been investigated for TAT, oligolysine, HSV-1 VP22, oligoarginine, Antp, (reviewed in Ref. [26]), zinc coordinated oligotyrosine peptides [27] and recently for TP10, pVEC and polyproline helix SAP [28]. A tetravalent presentation of deca-arginine fused to the p53 protein was shown to improve delivery efficiency even at low concentrations without increasing toxicity [29]. In the latter study, this increased activity was associated with enhanced interactions with cell surface heparan sulfates. However, these multivalent arrangements were either based on globular scaffolds or branched dendrimers, geometries that confine the area of interaction with the membrane components of the cell. To be effective for promoting uptake, a stretch of arginines has to be present. A dispersed presentation of individual arginines on a polymer results in considerably reduced uptake also at higher charge density [30]. Overall, the multivalent geometries that have been investigated so far for CPPs are more restricted than those addressed for antimicrobial peptides for which presentation along linear scaffolds has also been investigated, already [31].

In all these applications, the multivalent CPPs were well tolerated, showing little signs of toxicity. Also, individual oligoarginine peptides are generally well tolerated to concentrations in the mean micromolar range [11,24].

Beyond yielding a benefit in efficiency, so far, the multivalent display of CPPs has yielded little insights into the molecular mechanisms triggering import. Also, no functional characteristics were reported that differed greatly for those of the individual CPPs. As for individual CPPs, it has been proposed that the multivalent systems crosslink glycosaminoglycans followed by endocytosis [32]. This may be due to the globular nature of these structures that renders them very similar to CPPs linked to macromolecules.

Therefore, in the present study we compared a multivalent configuration of nona-arginine (R9) in which on average five copies of the CPP were coupled to a linear and flexible dextran backbone (Dex-$(R9)_5$) to the monovalent R9 counterpart. We hypothesized that in comparison to multivalent displays on globular structures, this configuration would result in contact of the molecule with a larger surface area of the plasma membrane or in a structurally adaptive binding due to the flexibility of the dextran backbone. In particular, we hoped that this configuration would shed further light into the structural requirements for triggering the rapid sphingomyelinase-dependent uptake mechanism. All data presented so far, indicated that this import route is restricted to free CPPs or CPPs conjugated to small molecular weight cargo [9,10].

Next to addressing uptake and toxicity for HeLa and Jurkat cells we also included human erythrocytes in our studies. These cells lack endocytosis and should therefore reveal to which degree a membrane-disruptive activity is a function of the conjugate–membrane interaction or the triggering of a cellular response. Since multivalency can generate strong interactions for low affinity binders, we also addressed whether inside the cell the multivalent display of R9 leads to the disruption of protein–protein interactions. Our results demonstrate that the multivalent display strongly enhances interactions with the plasma membrane. The restriction of toxicity to cells that show uptake demonstrates that toxicity is a consequence of the reaction of the cells to these conjugates. Interactions of the conjugates with the plasma membrane alone are insufficient to evoke strong toxicity.

2. Materials and methods

2.1. Reagents

Nona-arginine (R9) with an amidated C-terminus and an N-terminal carboxyfluorescein was purchased from EMC microcollections (Tübingen, Germany). Dex-$(R9)_5$ was synthesized using a 10 kDa dextran (Dex) backbone comprising on average of 62 glucose monomers. Carboxyethyl groups were introduced using acrylamide followed by amide hydrolysis to form 2-carboxyethyl dextran (CED). *N*-(2-aminoethyl)maleimide was synthesized and coupled to the modified polymer. Using maleimide-thiol coupling, in a single step *N*-cysteinyl-lysinyl-5(6)-carboxyfluorescein and *N*-cysteinylnona-arginine amide were coupled to the modified dextran achieving an average loading of five nona-arginine peptides and one fluorophore per polymer as determined by quantitative amino acid analysis and NMR [22]. Dex-$(R9)_5$ had a final molecular weight of 22 kDa (for details see SI, Figure S1.1 and S1.2). Dex and CED were used as negative controls. Imipramine, resazurin and Tween-20 were from Sigma-Aldrich (Zwijndrecht, the Netherlands). Propidium iodide and Alexa-647-labeled Annexin-V were from Invitrogen (Eugene, USA) and Ficoll-Paque from GE Healthcare (Uppsala, Sweden). Complete Ringer (pH 7.4) solution was prepared using 32 mM HEPES, 125 mM NaCl, 5 mM glucose, 5 mM KCl, 1 mM $MgSO_4$, 2.5 mM $CaCl_2$.

2.2. Tissue culture

Jurkat T cell leukemia cells (ACC-282, DSMZ, Braunschweig, Germany) and HeLa cells (CCL-2, ATCC, LGC Standards, Wessel, Germany) were cultured in RPMI1640 with stable glutamine and 2.0 g/L $NaHCO_3$ (PAN Biotech, Aidenbach, Germany) supplemented with 10% heat inactivated fetal bovine serum (FBS; PAN Biotech). Cells were maintained at 37 °C in a humidified incubator containing 5% CO_2. Jurkat cells were passaged every 2–3 days when the cells had grown to a density of approximately $4 * 10^5$ cells/mL while HeLa cells were passaged every 2 days at around 80%–90% confluency.

2.3. Confocal microscopy

Confocal laser scanning microscopy was performed on a TCS SP5 confocal microscope (Leica Microsystems, Mannheim, Germany) equipped with an HCX PL APO 63x 1.2 N.A. water immersion lens. Cells were maintained at 37 °C on a temperature-controlled microscope stage. For multichannel recordings with propidium iodide (PI) or Annexin-V in addition to the labeled R9 or Dex-$(R9)_5$, images were recorded using the 488 nm line of an argon-ion laser and a HeNe 561 or 633 nm laser. To avoid crosstalk, fluorescence was recorded sequentially where necessary.

2.4. Dex-$(R9)_5$ uptake

HeLa cells ($4 * 10^4$/well) were seeded in 8-well microscopy chambers (Nalge Nunc International, New York, USA), 24 hours prior to peptide addition. Cells were incubated with 4 μM Dex-$(R9)_5$ or 20 μM R9 in RPMI 1640 supplemented with 10% FBS (heat inactivated) for

20 minutes. For assessing the effect of imipramine on peptide uptake, cells were pre-incubated for 45 minutes with 30 μM imipramine in RPMI 1640 without serum. For subsequent incubation with peptide, 30 μM imipramine was co-incubated with peptide in medium containing 10% FBS. Cells were washed twice with medium. To check for membrane-integrity as well as cell viability, cells were incubated with 5 μg/mL PI and immediately imaged by microscopy. For studies in Jurkat cells, 200 μL of a 5 * 10^5 cells/mL Jurkat cell suspension in RPMI 1640 without phenol red and 10% FBS were transferred per well into 8-well microscopy chambers coated with a 20 μg/mL fibronectin solution in PBS for 30 minutes at room temperature (RT). At time point $t = 0$, 5 μM or 10 μM of R9 or 1 μM or 2 μM of Dex-$(R9)_5$ were added to the wells.

2.5. Image enhancement

Image J (version 1.46j, freeware, NIH) was used to modify brightness and contrast of the confocal microscopy images.

2.6. Image quantification

Image J (version 1.46j, freeware, NIH) was used to analyze the confocal microscopy images. Images were first smoothened and then converted into a binary mask using thresholds for fluorescence intensity and size. This mask was used to extract cell-associated fluorescence in the original background-corrected images. To separate adjacent cells a watershed function was applied to the binary mask. Mean intensities (represented as intracellular fluorescence) were measured from all cells within one image frame (at least 50 cells were analyzed).

2.7. Cytotoxicity assay

HeLa cells (7.5 * 10^3 cells/well) were seeded in 96-well microtiter plates and grown overnight. The next day, cells were treated with varying concentrations of R9/Dex-$(R9)_5$/Dex/CED for 24 hours at 37 °C. Cell viability was measured using the resazurin assay. Resazurin is a non-fluorescent dye that is reduced to the highly fluorescent resorufin by metabolically active cells [33,34]. Cells were incubated with resazurin (100 μg/mL) for 4 hours. Fluorescence was read with a Synergy 2 single-channel microplate reader (BioTek Instruments, Winooski, USA). Percentage cell viability was calculated as $[(Ti - T0)/(C - T0)] \times 100$ for concentrations in which $Ti \geq T0$ and $[(Ti - T0)/T0] \times 100$ for concentrations in which $Ti < T0$. Ti is the fluorescence of the test-well after a 24-hour period of exposure to the treatment, T0 is the fluorescence at time zero (i.e. before addition of compounds) and C is the fluorescence after 24 hours of cell seeding. This parameter can have values from +100 to −100 [35].

2.8. Effect of Dex-$(R9)_5$ on erythrocytes

Blood was drawn from healthy volunteers. The study was performed following the guidelines of the local medical ethical committee and in accordance with the declaration of Helsinki. Written informed consent was obtained from all blood donors participating in this study. To isolate erythrocytes, fresh blood was centrifuged at 1500×g for 10 minutes. Erythrocyte pellets were washed twice with calcium-free Ringer to prevent complement activation and once with complete Ringer. Erythrocytes were resuspended in 100 μL Ringer and diluted to 1 million cells/well in chambered coverslips. R9 or Dex-$(R9)_5$ were added to the cells in an equal volume of Ringer at the indicated concentrations and imaged by time lapse confocal microscopy. Alexa-647-labeled Annexin-V was also added at a dilution of 1:25. Cells were manually counted to quantify exposure of phosphatidylserine, changes in morphology and lysis.

2.9. Impact of Dex-$(R9)_5$ on protein–protein interactions

In order to induce activation-dependent protein complex formation, Jurkat cells were treated with 0.5 mM of the broad-range phosphatase inhibitor pervanadate (PV) in HBS or as a control with HBS for 10 minutes at 37 °C. Cell lysates were prepared by suspending 1 million cells per subarray in 50 μL lysis buffer (1% Triton X-100, 50 mM *n*-octyl-D-glucopyranoside (Fluka, Taufkirchen, Germany), 20 mM Tris, 1 mM EDTA, 150 mM NaCl, 1 mM Na_3VO_4, pH 7.5, and complete protease inhibitor cocktail (Roche Applied Science, Mannheim, Germany)). *N*-octyl-D-glucopyranoside ensured the efficient extraction of signaling proteins from lipid rafts. After lysis on ice for 1 hour, the crude lysates were cleared by centrifugation at 20,000×g at 4 °C for 15 minutes. Afterwards, 5 μM R9 or 1 μM Dex-$(R9)_5$ was added to cell lysate. Finally, lysates were incubated on microarrays as described below. Peptide microarrays presenting known interaction motifs for proteins involved in T cell signaling were prepared as described before [36]. One microarray substrate carried 16 identical subarrays. For incubation of these subarrays with different samples a 16-well clip-on frame (ProPlate Multiarray System, Grace Biolabs, Molecular Probes, Eugene, OR, USA) was mounted onto the microarray slides. Microarrays were incubated with 50 μL of lysate from 1 million cells per subarray for 1 hour at 4 °C and washed three times with washing buffer (PBS, 0.05% (wt/vol) BSA, 0.05% (wt/vol) Tween-20). For the detection of bound protein by indirect immunofluorescence, microarrays were incubated with 2 μg/mL primary antibody (α-PLCγ1, Santa Cruz Biotechnology, Heidelberg, Germany, sc-81; α-LAT, Millipore 05-770, Schwalbach, Germany) diluted in washing buffer for 15 minutes at RT and washed three times with washing buffer. Afterwards, microarrays were incubated with 1 μg/mL secondary goat-anti-rabbit antibody conjugated with Alexa-633 and goat-α-mouse secondary antibody conjugated with Alexa-546 (A21070, A11003, Invitrogen) for 10 minutes at RT followed by a final washing step with washing buffer. As a negative control, one subarray was immunostained without incubation with lysate. Finally, microarrays were dried with nitrogen and scanned (ProScanArray, PerkinElmer Life Sciences, Waltham, MA, USA). Processing of the signals occurred as described previously using ArrayPro Analyzer (Media Cybernetics, Silver Spring, MD, USA) [36]. Signals on microarrays were obtained by subtraction of the median signal of a local ring-shaped background from the mean of signal intensities on a peptide spot.

3. Results

3.1. Dex-$(R9)_5$ exhibits sphingomyelinase-dependent uptake and nucleolar staining

Previous work on multivalent cationic peptides and protein transduction domains elucidated that multivalency greatly improves cellular import of these conjugates [29]. Uptake occurred by endocytosis, consistent with the general assumption according to which macromolecular CPP-complexes and conjugates are taken up along this route and direct translocation and rapid cytoplasmic uptake are restricted to free CPPs and CPPs conjugated to small molecular weight cargo [9,10]. However, so far, multivalent configurations were nanoparticulate, potentially restricting the ability of these molecules to engage with larger areas of the plasma membrane. Therefore, we here synthesized a highly flexible multivalent CPP conjugate by coupling on average five copies of nona-arginine to a 10-kDa dextran backbone. A fluorescein moiety was introduced to monitor the cellular distribution and uptake.

HeLa cells were incubated with 20 μM R9 or 4 μM Dex-$(R9)_5$, corresponding to the same concentration of CPP and the distribution of fluorescence was observed by confocal microscopy in living cells. As reported before, at this concentration R9 exhibited a uniform homogeneous staining of cells with only few endocytic vesicles [11] (Fig. 1, also SI, Figure S2). This is the typical distribution of fluorescence

observed for sphingomyelinase-dependent import through nucleation zones [10,11]. Also for Dex-$(R9)_5$ cells showed an intense cytoplasmic fluorescence, however, this fluorescence was distributed less homogenously than for R9 and also showed a distinct nucleolar staining as was observed for the D-Amino acid analog of R9 [14]. Areas of more intense fluorescence were reminiscent of nucleation zones. Also, cell shapes were more irregular for Dex-$(R9)_5$-treated cells than for cells incubated with free peptide, suggesting a stronger membrane-perturbing effect of the multivalent conjugate. Interestingly, cell-associated fluorescence for Dex-$(R9)_5$ was about the same as for R9 (Fig. 1B). Considering, that one conjugate carried one fluorophore for five peptides, this indicates that on a per-peptide basis, uptake was in about the same range (maximum five fold higher per peptide) than for R9.

Sensitivity to imipramine which acts as an inhibitor of acid sphingomyelinase was identified as a characteristic of nucleation zone-dependent uptake [10]. However, as detailed above this route of uptake was limited to free CPPs or CPPs conjugated to small cargos [9,10]. A polymer-conjugate of similar size but with only 3 nona-arginines was unable to enter via this route [10,37]. To investigate whether Dex-$(R9)_5$ nevertheless exploited this mechanism or whether uptake occurred as a consequence of membrane disruption, uptake was assessed in the presence of imipramine. Imipramine abolished cytoplasmic fluorescence of both, R9 and Dex-$(R9)_5$ in a major part of cells supporting a role of sphingomyelinase-dependent uptake in both cases (Fig. 1, SI Figure S2). To exclude that the reducing effect was due to an interference of the imipramine with the peptides/conjugate at the plasma membrane, we compared the effect of a pre-incubation with imipramine with the one of a pre- and co-incubation. Indeed, in the latter case the reduction was stronger demonstrating that some direct interference occurs (SI, Figure S3).

Considering the more irregular cell shape for the Dex-$(R9)_5$-treated cells we also probed for membrane damage which does not occur for sphingomyelinase-dependent uptake [11]. Cells were exposed to conjugates for 20 minutes and after washing PI was added to monitor changes in membrane integrity. For the multivalent conjugate there was a loss of membrane integrity for some cells (Fig. 2). Remarkably, the number of PI-positive cells was decreased by the presence of imipramine indicating that membrane damage is a consequence of uptake rather than the interaction of the conjugate with the plasma membrane (Fig. 2). This increased membrane-disruptive potential was also reflected by a higher reduction in cell viability over a 24-hour

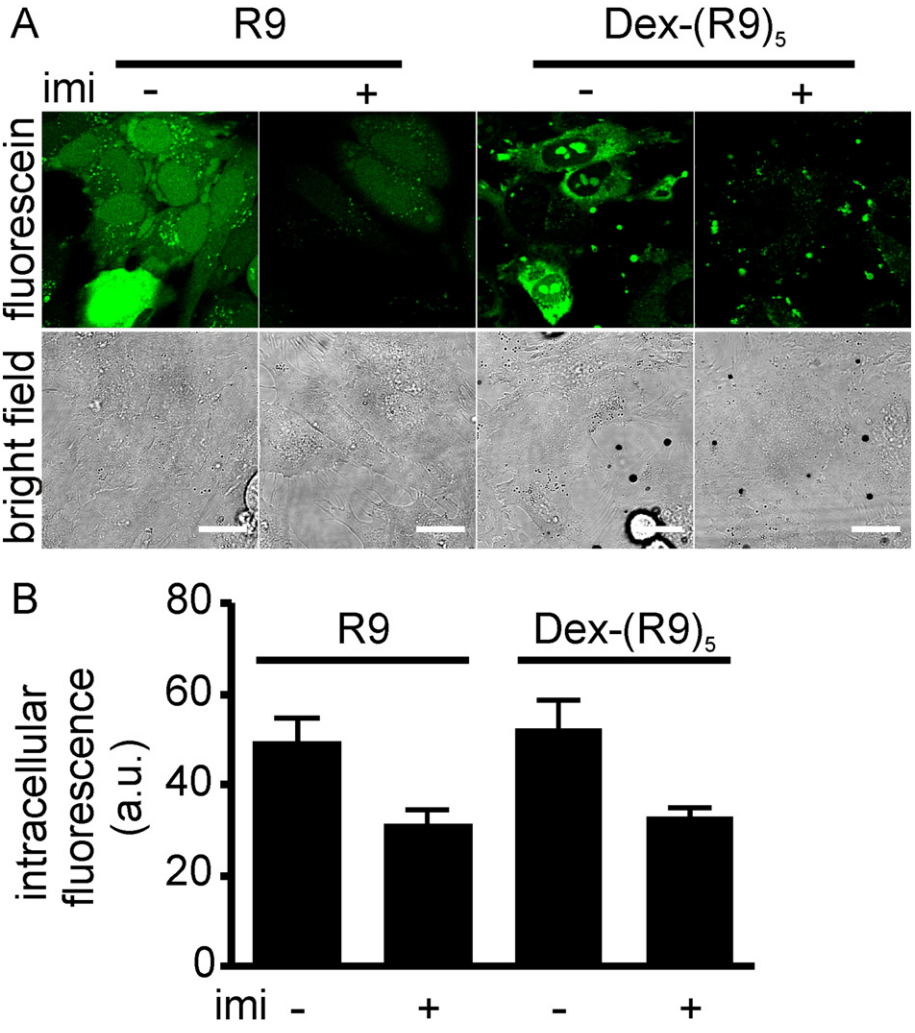

Fig. 1. Cellular distribution and imipramine-sensitive uptake of Dex-$(R9)_5$. (A) Following a 45 minute pretreatment with/without imipramine (imi) in serum-free RPMI, HeLa cells were incubated with 20 μM R9 or 4 μM Dex-$(R9)_5$ for 20 minutes at 37 °C in the presence or absence of 30 μM imipramine followed by washing and imaging with confocal microscopy. Microscopy settings for image acquisition of all samples were adjusted for R9 to avoid saturation. One confocal slice is shown for all the microscopy images. Scale bars correspond to 20 μm. One representative experiment of at least three experiments is shown. Homogenous staining of R9 is observed in 70% of cells (for whole field-of-view of images see SI, Section S2, Figure S2). Brightness and contrast have been adjusted for visualization purposes using the same parameters for fluorescence images and parameters to yield the best possible result for transmission images. (B) Imipramine-sensitive uptake quantified from A (raw, unmodified images); at least 50 cells were counted. Error bars represent S.E.

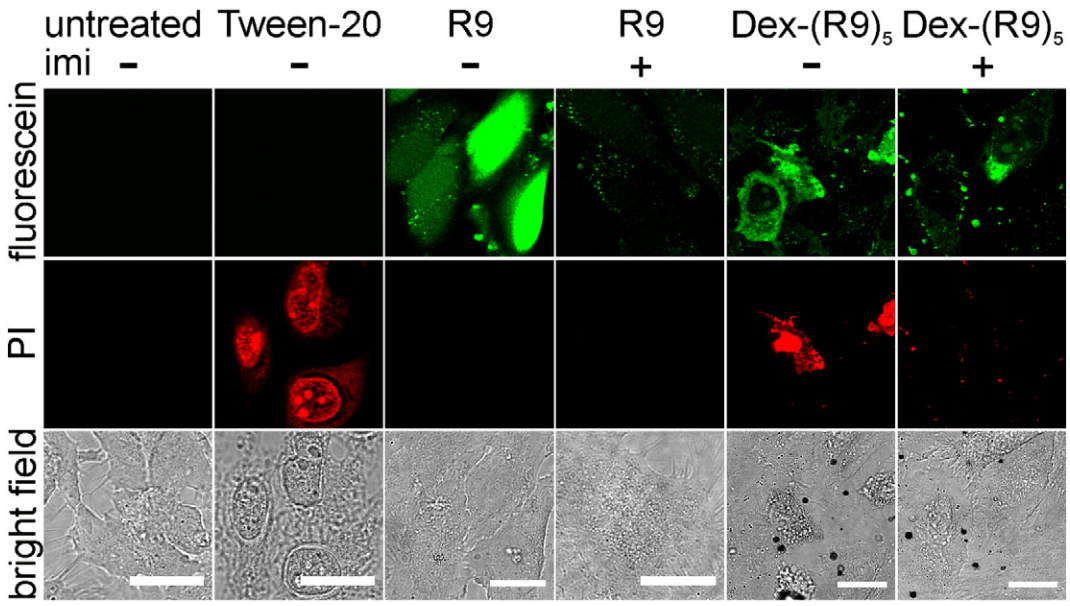

Fig. 2. Uptake of Dex-$(R9)_5$ is associated with only partial loss of membrane integrity. HeLa cells were treated with 4 μM Dex-$(R9)_5$ or 20 μM R9 for 20 minutes at 37 °C in the presence or absence of 30 μM imipramine (imi) as stated before. After washing, PI (5 μg/mL) was added and cells were imaged without any further washing step by confocal microscopy. Tween-20 (0.25%) was used as a positive control for membrane disruption. Scale bars correspond to 20 μm. Brightness and contrast have been adjusted for visualization purposes using the same parameters for fluorescence images and parameters to yield the best possible result for transmission images.

incubation (Fig. 3). A strong reduction in cell viability was noticed for 1 μM Dex-$(R9)_5$ (corresponding to an overall peptide concentration of 5 μM) compared to 11 μM R9 over 24 hours. Dex and CED, which were used as negative controls, did not show any significant toxicity indicating that neither the native nor the carboxyethylated dextran backbone were responsible for the toxicity of Dex-$(R9)_5$.

HeLa cells have a high density of heparan sulfates and other negatively charged oligosaccharides [38] that serve as binding sites for arginine-rich peptides [39]. We were therefore interested to assess the impact of the linear, multivalent Dex-$(R9)_5$ conjugate on Jurkat T cell leukemia cells that express significantly lower levels of heparan sulfates [38]. At 5 μM (Fig. 4A and SI movie S4-M1), over the time course of the experiment, R9 showed only internalization in a few cells with no signs of toxicity. At 10 μM (Fig. 4B and movie S4-M2), R9 fluorescence rapidly entered the cytoplasm reminiscent of nucleation zone-dependent uptake [11]. For the free peptide, uptake occurred in the absence of visible membrane staining. In contrast, Dex-$(R9)_5$ (Fig. 4C and D and SI movies S4-M3, S4-M4), already at a concentration of 1 μM with respect to backbone caused massive membrane staining and cell death accompanied by formation of membrane blebs. Control CED had no effect on cell viability (Fig. 4E and SI movie S4-M5).

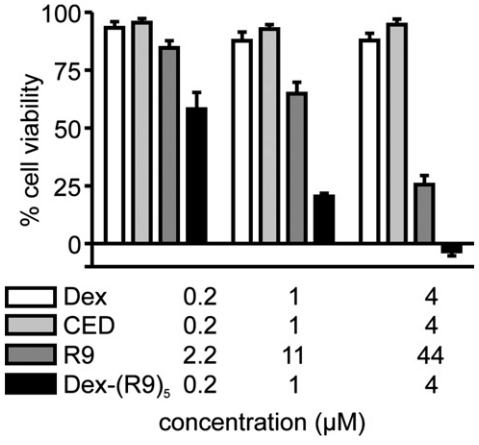

Fig. 3. Multivalency of nona-arginine in Dex-$(R9)_5$ increases toxicity. HeLa cells were treated with the indicated concentrations of Dex-$(R9)_5$ (with respect to the polymer backbone) for 24 hours and cell viability was determined using a resazurin assay in comparison to R9. CED (carboxyethyl dextran) and Dex (native dextran) were used as controls. Data represents average ± SEM of three independent experiments, each carried out in triplicate, which means $N = 9$.

3.2. Dex-$(R9)_5$ but not R9 binds to erythrocyte membranes and induces cell aggregation

Concomitant with increased toxicity, for Dex-$(R9)_5$ we observed an increased membrane staining which was absent for R9. Two possible explanations were considered for this membrane staining. First, the multivalent display of guanidino-groups could afford sufficient avidity for interaction with the plasma membrane also in the absence of a massive disturbance. Second, staining could be a consequence of the membrane-disruptive effect of the conjugate, leading to exposure of negatively charged phosphatidylserine that would then in turn lead to a membrane accumulation of the peptide. In this second case, it would be interesting to learn whether disruption was again a function of the peptide alone, or of the cellular response to the peptide. In order to distinguish these mechanisms, we employed erythrocytes as a model system. In contrast to nucleated cells, erythrocytes do not exhibit endocytosis. Cationic amphipathic, membrane-active peptides like mastoparan [40], gramicidin S [41], mellitin [41] and several other drugs [42] have been shown to cause shape changes and cell lysis in erythrocytes. For CPPs only few studies about the impact on erythrocytes exist. One study addressed the uptake of α- and β-oligoarginines in normal versus parasite-infected erythrocytes [43] demonstrating that both types of oligoarginines did not enter healthy erythrocytes but only the parasite-infected ones. TAT only showed activity in combination with a phototoxic effect [44].

Erythrocytes were incubated with Dex-$(R9)_5$ in the presence of fluorescently labeled Annexin-V and the impact on erythrocyte morphology and phosphatidylserine exposure was determined by time lapse confocal microscopy (Figs. 5A, SI Figure S5.1 and movie S5-M6). The multivalent conjugate bound to the membrane almost immediately after addition. For 37% of the cells (3 independent experiments with 605 cells in total) this binding was followed by phosphatidylserine exposure (detected by binding of Annexin-V), indicating that disruption of

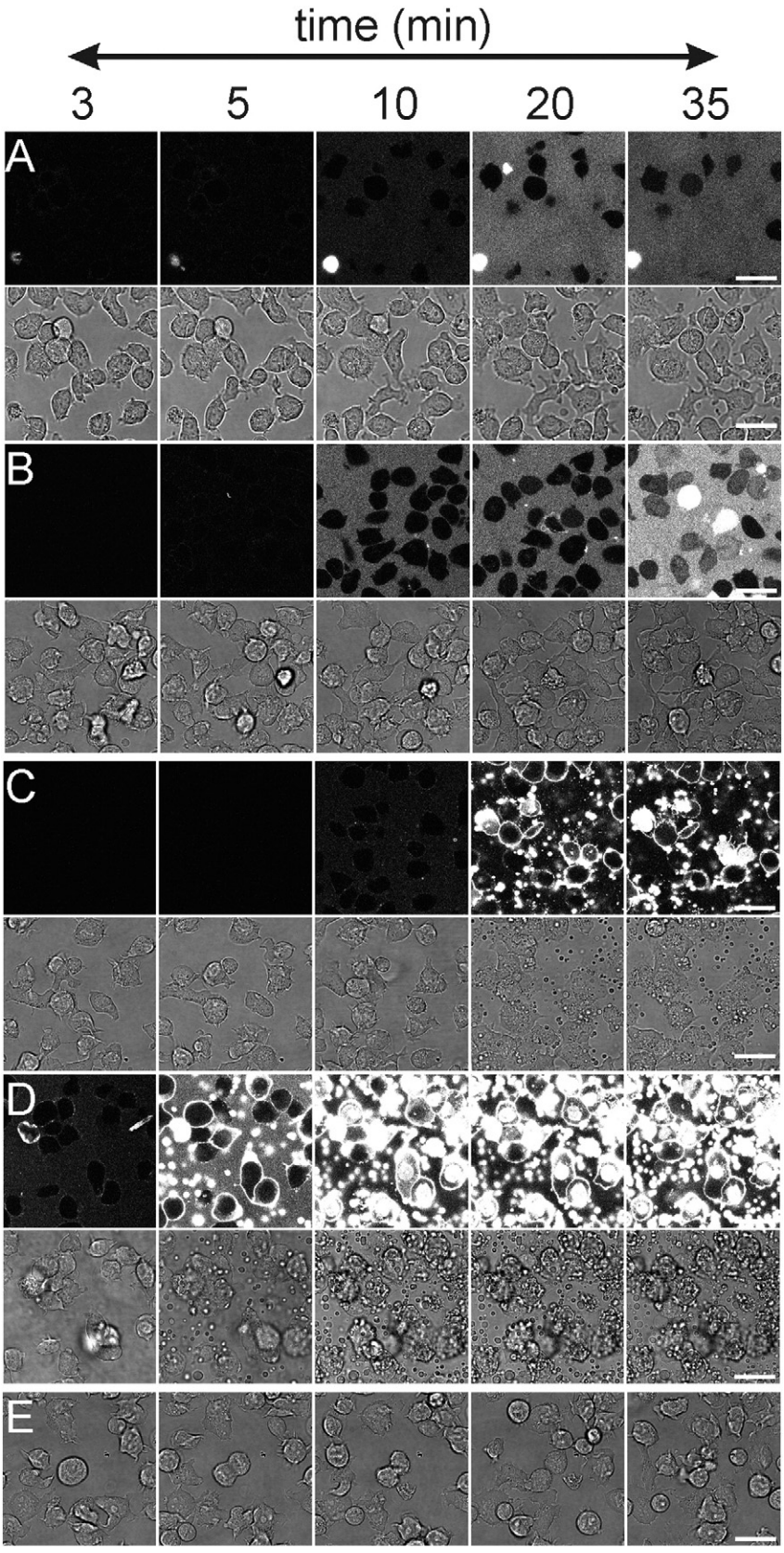

Fig. 4. Time lapse microscopy of the membrane-disruptive behavior of Dex-$(R9)_5$ in Jurkat cells. Jurkat cells were exposed to (A) 5 μM R9, (B) 10 μM R9, (C) 1 μM Dex-$(R9)_5$ and (D) 2 μM Dex-$(R9)_5$ at 37 °C and fluorescence and transmission recorded with 2 images/min. Concentrations of Dex-$(R9)_5$ were with respect to the polymer backbone. CED of 2 μM (E) was used as control. Peptide/conjugate was added at the time of image acquisition by careful pipetting into the sample. The start of exposure of cells to peptide/conjugate is visible from the increase in fluorescence outside the cells. Scale bars correspond to 25 μm. Also see SI, movies S4-M1 to M5.

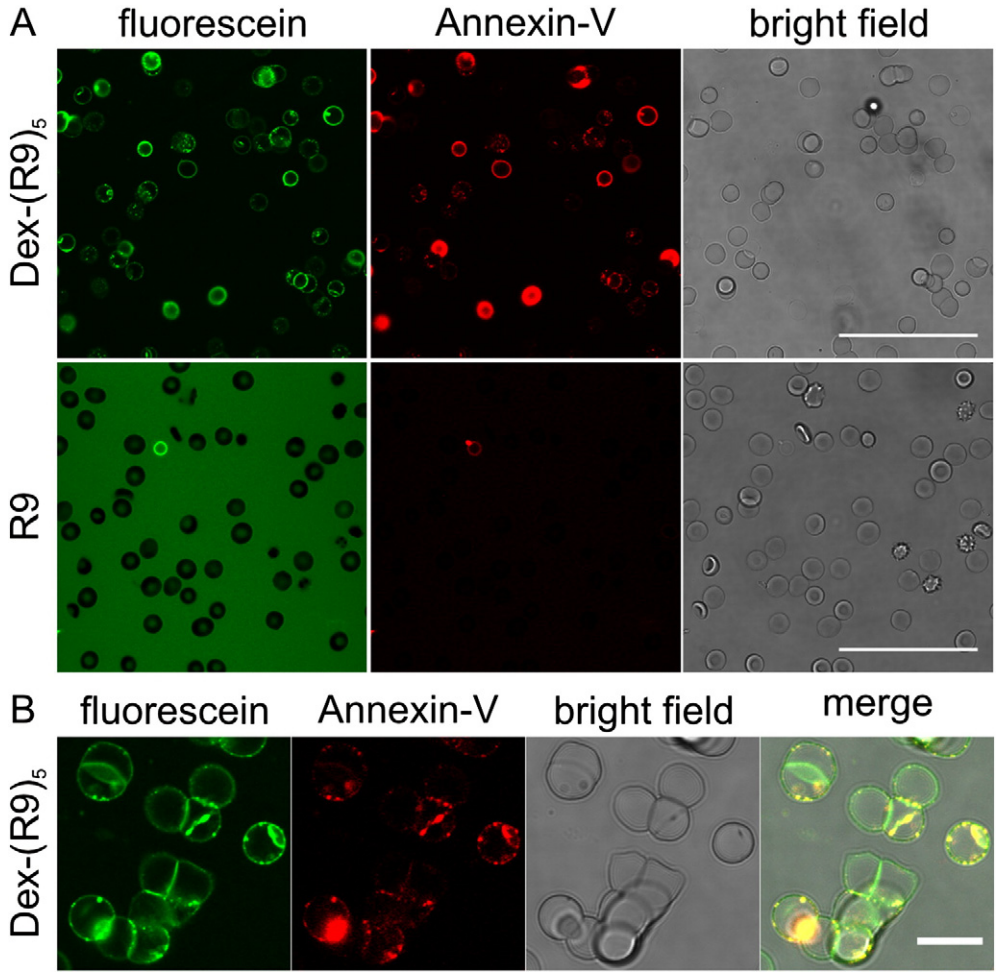

Fig. 5. Dex-$(R9)_5$ induces erythrocyte aggregation and phosphatidylserine exposure. (A) 0.6 μM Dex-$(R9)_5$ and 6 μM R9 were added to erythrocytes in Ringer and imaged by confocal microscopy at 37 °C after 20 minutes. Annexin-V was also added to cells at a dilution of 1:25 to stain for phosphatidylserine. Scale bars correspond to 50 μm. (B) Erythrocyte aggregates formed after the addition of 0.6 μM Dex-$(R9)_5$. The scale bar corresponds to 10 μm. Also see SI movies S5-M6 and M7.

membrane polarity was a potential consequence but not the cause of strong binding of the conjugates. Phosphatidylserine exposure was followed by disruption of membrane integrity as visible by entry of fluorescence into the cytoplasm. By 20 minutes, 9% of the cells were lysed. Interestingly, within the first 2 minutes erythrocytes also formed aggregates (Fig. 5B, SI Figure S5.1, movie S5-M6) that incorporated 50% of cells at 0.6 μM of Dex-$(R9)_5$. In contrast, addition of 6 μM R9 to erythrocytes in Ringer exhibited weaker membrane staining and did not show any aggregates (Fig. 5, SI Figure S5.2 and movie S5-M7). No cell entry was observed. Moreover, only a minor percentage of cells (around 4% from 2 different experiments, 595 cells in total) showed shape changes and formed echinocytes (by 20 minutes) without exposure of phosphatidylserine (SI Figure S5.2 and movie S5-M7). CED, the dextran backbone control, induced no changes in erythrocyte morphology (SI, Figure S6). To explore to which degree the membrane aggregating behavior of Dex-$(R9)_5$ would extend to potential in vivo applications, erythrocytes were also exposed to the conjugate in the presence of human serum. Serum completely neutralized the effects of Dex-$(R9)_5$ on erythrocytes observed in Ringer (SI, Figure S6).

3.3. Both, Dex-$(R9)_5$ and R9 interfere with protein–protein interactions involved in early T-cell signal transduction

The observations for Jurkat cells and erythrocytes demonstrated that the multivalent display of R9 strongly potentiated the capacity to interact with lipid membranes independent of the presence of heparan sulfates. Clearly, on the linear backbone, multivalency yielded sufficient avidity to support interactions with the lipid head groups. Given a recent report of interactions of arginine-rich peptides with microfilaments [45], we were interested to learn whether multivalency also conferred an increased capacity to interfere with protein–protein interactions. To this end, we took advantage of a peptide-based microarray approach which we had used before to probe in parallel for signaling-dependent changes in the formation of protein complexes in Jurkat T cells [36]. The peptide arrays comprised a collection of phosphotyrosine-containing and proline-rich peptides which interact with SH2 and SH3 domains that play a major role in the organization of signaling pathways [46,47]. Binding of proteins from cell lysates was probed by indirect immunofluorescence. We opted for PLCγ1 [48,49] and the scaffold protein LAT [50,51], two important players in early complex formation within T cell signaling, as indicators for a possible impact on protein–protein interactions. PLCγ1 can bind to peptides on the microarray via its SH2 and SH3 domains. In contrast, LAT can only bind as part of a protein complex as it has no suitable domains to directly engage in interactions with peptides on the array. LAT should therefore be a sensitive indicator for changes in protein–protein interactions. In order to trigger signaling events and induce formation of protein complexes, Jurkat cells were stimulated with the broad-range phosphatase inhibitor pervanadate [52] or as a control for resting cells treated with HBS only. Pervanadate leads

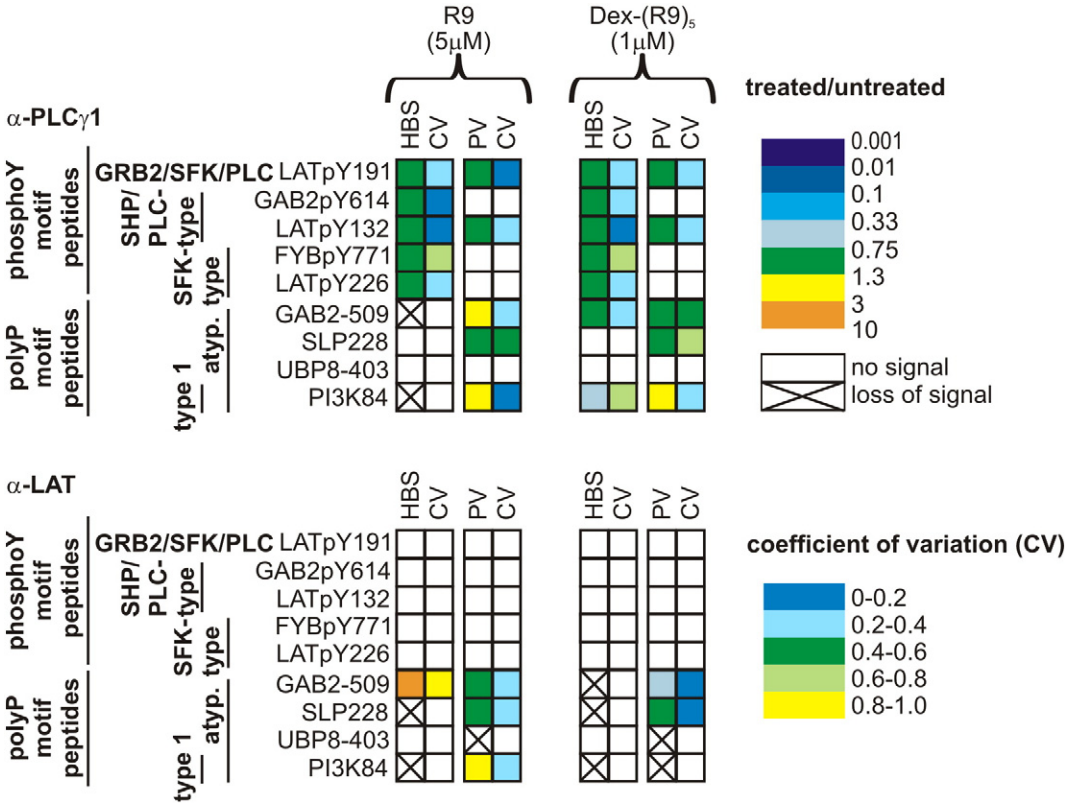

Fig. 6. Impact of R9 and Dex-$(R9)_5$ on protein–protein interactions. Peptide microarrays were incubated with Jurkat cell lysates in the presence and absence of free R9 or the conjugate. Colored squares indicate ratios of signals of treated cell lysates over untreated lysates on respective peptides and respective coefficients of variation (CV). A cross relates to a signal that was lost in the presence of peptide or conjugate. Cells were either resting (HBS) or stimulated with the broad-range phosphatase inhibitor pervanadate (PV). All data are mean values of three independent experiments. Shown are those nine out of thirty one peptides on the arrays for which signals could be observed.

to the phosphorylation of tyrosines and as a consequence to SH2 domain-mediated complex formation. Addition of R9 and Dex-$(R9)_5$ caused the loss of several signals on proline-rich peptides but not on phosphotyrosine-containing peptides (Fig. 6). Also LAT was affected more strongly than PLCγ1 consistent with the indirect binding of LAT as part of a protein complex which provides several points for interference with the interaction. However, there was little difference between R9 and Dex-$(R9)_5$.

4. Discussion

Oligoarginines have gained ample attention as CPPs due to their high internalization efficiency [24,25,53,54]. An increase of the valency of the guanidino-group through a multivalent display of oligoarginines further increases uptake efficiency [29]. So far, investigations of multivalency have focused on uptake efficiency and intracellular trafficking of globular molecular geometries [26]. For example, the tetravalent display of the TAT CPP increased uptake efficiency by 1000-fold. Interestingly, to this point there were no indications that the multivalent configuration conferred qualitatively new characteristics to the interaction of these molecules with cells.

In this study, we linked on average five nona-arginine CPPs to a linear dextran backbone. With this linear geometry, in a fully stretched conformation this multivalent construct can engage plasma membrane over a length of at least 25 nm (the dextran polymer backbone, Dex, exhibits this length in the extended conformation [22]) and a width of 7 nm (two fully extended R9), yielding a maximal contact area of 175 nm^2. In comparison, a streptavidin molecule which has been used as a globular scaffold has a diameter of 5 nm which would be extended by fully stretched peptides to 12 nm and thus an equivalent contact area of 144 nm^2. This similarity in size indicates that the observed differences must to a large extend be a consequence of the flexibility of the dextran backbone.

Remarkably, as derived from quantitative image analysis, uptake of the conjugate, when related to peptide, was enhanced by a factor of five at most in comparison of the free peptide. Therefore, this linear arrangement of oligoarginines falls behind what was observed for the globular configurations. However, very interestingly, this construct showed the same imipramine-sensitive cytoplasmic uptake as the free peptide, in spite of a total molecular weight of 22 kDa (CED + peptides). So far, observations by us [10] and others [9] had shown that this uptake is restricted to small molecules only. In fact, elongation of nona-arginine by only a heptapeptide strongly reduced the efficiency of this uptake route. The molecular details of the nucleation zone-dependent uptake still remain elusive. Based on the sphingomyelinase dependence and the formation of ceramide, a lipid that forms membrane microdomains [47], we proposed a model according to which peptides enter along domain boundaries in a non-disruptive manner. Even though still speculative in nature, the uptake that we observed here demonstrates that a continuous display of arginines along a flexible, linear scaffold enables passage through these domain boundaries also for larger molecules. It is tempting to assume that the peptides act like pearls on a string. The ability to also drive larger molecules across the membrane by this mechanism further supports a privileged role for arginines for partitioning into lipid bilayers. Furthermore, local arginine density instead of the absolute concentration of molecules is decisive in triggering this uptake route as in both cases the concentration of nona-arginine was 20 μM.

Nevertheless, the nucleation zone dependent entry was superimposed by a stronger membrane-perturbation, demonstrating that a covalent linkage to a linear scaffold is not equivalent to the addition as independent molecules. On HeLa cells, already at a peptide

concentration of 1 μM the multivalent conjugate showed significant long-term toxicity over a period of 24 hours. This membrane-disruptive capacity was even enhanced on Jurkat cells. Jurkat cells possess only little glycocalyx [38]. While we cannot exclude that the glycocalyx present on Jurkat cells mediates the observed interaction, the strong membrane perturbation induced by the conjugate on the Jurkat cells and enrichment in the plasma membrane indicates that the peptide exerts a much stronger perturbating effect on the lipid bilayer. It is reasonable to assume that this is a consequence of the peptide gaining more readily access to the lipid bilayer and interacting with lipid head groups. Exposure of negatively charged phosphatidylserines further enhances this interaction. One may also envision that an initial local exposure of phosphatidylserine further promotes membrane association and thus membrane perturbation.

It is notable that the massive membrane staining was restricted to Jurkat cells and also that for Jurkat cells, the conjugate did not gain access to the cytoplasm. In our opinion, the most likely way of reasoning is that in Hela cells the conjugate induces rapid uptake and that interactions with the glycocalyx shield the lipid bilayer, while for Jurkat cells, in the absence of a pronounced glycocalyx the perturbation of the lipid bilayer dominates and the peptide is sequestered by the plasma membrane and therefore not able to reach the cytosol.

Our results differ from those of Kawamura et al. [29], who showed that the tetravalent display of deca-arginine at the N-terminus of the p53 tetramerization domain did not confer any toxicity to CHO cells at a peptide concentration of up to 25 μM for 4 hours. This discrepancy suggests that a conformationally constrained arrangement of oligoarginines as part of a macromolecule has a lower membrane-disturbing potential, an observation in line with the absence of toxicity of CPP-functionalized quantum dots [55] and nanoparticles [56]. However, very interestingly, the capacity to engage in interactions with the lipid bilayer by itself was not sufficient for causing severe toxicity. The dextran conjugate also strongly bound to and even cross-linked erythrocytes. While this led to exposure of phosphatidylserine in a considerable number of cells, there was no disruption of cells and massive lysis.

In contrast, at a concentration of 6 μM, R9 was completely indifferent to erythrocytes. These observations demonstrate that with a higher degree of multivalency, when linked to a linear scaffold, oligoarginine acquires fundamentally new characteristics. Several articles have reported on such aggregation behavior of erythrocytes being dependent on the size and concentration of polymers such as dextran and also on the surface charges on the erythrocyte membrane [57–59]. However, the minimum size of dextran reported to cause erythrocyte aggregation is 40 kDa at concentrations of 30–40 g/L corresponding to 750 μM-1 mM [57]. A smaller dextran with 20 kDa was not able to induce any aggregation up to a concentration of 120 g/L corresponding to 6 mM [57]. For Dex-$(R9)_5$ no cross-linking occurred in the presence of serum, indicating a strong serum binding of the conjugate that competed for membrane interactions [60] (SI, Figure S6). Erythrocytes do not possess endocytosis and also lack sphingomyelinase demonstrating that the increased toxicity for HeLa and Jurkat cells is a consequence of the reaction of the nucleated cells towards the conjugate rather than a membrane disruption caused by the physicochemical characteristics of the conjugate. This is also supported by the reduced membrane disruption for HeLa cells in which the sphingomyelinase-dependent uptake had been abolished by imipramine treatment.

Since arginine-rich CPPs have already been shown to interact with actin and stabilize stress fibers [45], we set out to test whether R9 and Dex-$(R9)_5$ also had an impact on molecular interactions inside the cell. We opted for our peptide microarray-based approach as it provides a straightforward means to probe for the perturbation of several interactions in parallel and furthermore also captures an impact on the formation of signaling complexes. Both R9 and the Dex-$(R9)_5$ conjugate had a similar disturbing effect on interactions mediated by proline-rich peptides. It is difficult to predict to which degree this disruptive potential will be significant in vivo. However, given the fact that polyvalency did not increase the disrupting behavior, we consider it highly unlikely that also at significantly higher concentrations R9 will severely disturb protein-protein interactions in cellular signaling. This is also in accordance with the fact that the massive cytosolic import that is observed for nucleation zone-dependent uptake does not cause any acute toxicity or perturbation of cell structure.

5. Conclusions

In summary, our analyses show that for arginine-rich CPPs multivalency on a linear scaffold affords a high avidity that critically affects the interaction with cellular membranes. As demonstrated for binding of R9 to erythrocytes, no binding is detected for the free peptide while strong binding and also cross-linking into erythrocyte stacks/aggregates occurs for the multivalent Dex-$(R9)_5$ conjugate. For HeLa and Jurkat cells, this multivalency strongly increases toxicity. The observed toxicity for both cell lines demonstrates that this increase in avidity is also observed for Jurkat cells with low levels of glycocalyx, indicating that interactions with lipids play a more prominent role. In addition, the membrane-disruptive behavior is a function of peptide uptake and not of the conjugate alone. These results clearly demonstrate that arginine-rich CPPs engage membrane structures just strong enough to trigger uptake while avoiding detrimental multivalent interactions that disturb membrane organization of larger areas.

Supplementary related to this article can be found online at http://dx.doi.org/10.1016/j.bbamem.2014.08.001

Synthesis of Dex-$(R9)_5$ (SI Figure S1.1, Figure S1.2, Table S1), whole field-view of cellular distribution and imipramine sensitive uptake of Dex-$(R9)_5$ in HeLa cells (SI Figure S2), effect of imipramine on peptide internalization (SI Figure S3), time lapse microscopy movies showing uptake in Jurkat cells (SI movies S4-M1 to M5), time lapse movies showing interaction of R9 and Dex-$(R9)_5$ with erythrocytes (SI Figure S5.1, S5.2 and movies S5-M6 to M7), confocal microscopy images showing the effect of human serum on binding behavior of Dex-$(R9)_5$ towards human erythrocytes (SI Figure S6).

Acknowledgments

The authors are thankful to all the blood donors for the erythrocyte experiments and to Dr. Carlo Tomelleri for help with erythrocyte/serum experiments. The authors also acknowledge Dr. Giel J. Bosman for helpful discussions. This work was supported by the Volkswagen Foundation (I/77 472) and the Deutsche Forschungsgemeinschaft (BR2443/5-1, RA895/4-1, and SFB 765). The funding sources have no role in study design; collection, analysis and interpretation of data; in writing of the report; and in the decision to submit the article for publication.

References

[1] M. Lindgren, M. Hallbrink, A. Prochiantz, U. Langel, Cell-penetrating peptides, Trends. Pharmacol. Sci. 21 (2000) 99–103.
[2] E. Snyder, S. Dowdy, Cell penetrating peptides in drug delivery, Pharm. Res. 21 (2004) 389–393.
[3] F. Milletti, Cell-penetrating peptides: classes, origin, and current landscape, Drug. Discov. Today 17 (2012) 850–860.
[4] S. Andaloussi, T. Lehto, I. Mager, K. Rosenthal-Aizman, I.I. Oprea, O. Simonson, H. Sork, K. Ezzat, D. Copolovici, K. Kurrikoff, J. Viola, E. Zaghloul, R. Sillard, H. Johansson, F. Said, P. Hassane, J. Guterstam, P. Suhorutsenko, N. Moreno, J. Oskolkov, U. Halldin, A. Tedebark, B. Metspalu, J. Lebleu, C. Lehtio, U. Smith, Lange, Design of a peptide-based vector, PepFect6, for efficient delivery of siRNA in cell culture and systemically in vivo, Nucleic. Acids. Res. 39 (2011) 3972–3987.
[5] L. Cantini, C. Attaway, B. Butler, L. Andino, M. Sokolosky, A. Jakymiw, Fusogenic-oligoarginine peptide-mediated delivery of siRNAs targeting the CIP2A oncogene into oral cancer cells, PLoS One 8 (2013) e73348.
[6] C. Watkins, D. Schmaljohann, S. Futaki, A. Jones, Low concentration thresholds of plasma membranes for rapid energy-independent translocation of a cell-penetrating peptide, Biochem. J. 420 (2009) 179–189.

[7] C. Jiao, D. Delaroche, F. Burlina, I. Alves, G. Chassaing, S. Sagan, Translocation and endocytosis for cell-penetrating peptide internalization, J. Biol. Chem. 284 (2009) 33957–33965.
[8] W. Verdurmen, R. Brock, Biological responses towards cationic peptides and drug carriers, Trends. Pharmacol. Sci. 32 (2011) 116–124.
[9] G. Tunnemann, R. Martin, S. Haupt, C. Patsch, F. Edenhofer, M. Cardoso, Cargo-dependent mode of uptake and bioavailability of TAT-containing proteins and peptides in living cells, FASEB. J. 20 (2006) 1775–1784.
[10] W. Verdurmen, M. Thanos, I. Ruttekolk, E. Gulbins, R. Brock, Cationic cell-penetrating peptides induce ceramide formation via acid sphingomyelinase: implications for uptake, J. Control. Release 147 (2010) 171–179.
[11] F. Duchardt, M. Fotin-Mleczek, H. Schwarz, R. Fischer, R. Brock, A comprehensive model for the cellular uptake of cationic cell-penetrating peptides, Traffic 8 (2007) 848–866.
[12] A. Ziegler, J. Seelig, Binding and clustering of glycosaminoglycans: a common property of mono- and multivalent cell-penetrating compounds, Biophys. J. 94 (2008) 2142–2149.
[13] I. Nakase, A. Tadokoro, N. Kawabata, T. Takeuchi, H. Katoh, K. Hiramoto, M. Negishi, M. Nomizu, Y. Sugiura, S. Futaki, Interaction of arginine-rich peptides with membrane-associated proteoglycans is crucial for induction of actin organization and macropinocytosis, Biochemistry. 46 (2007) 492–501.
[14] W.P. Verdurmen, P.H. Bovee-Geurts, P. Wadhwani, A.S. Ulrich, M. Hallbrink, T.H. Kuppevelt, R. Brock, Preferential uptake of L- versus D-amino acid cell-penetrating peptides in a cell type-dependent manner, Chem. Biol. 18 (2011) 1000–1010.
[15] J. Rothbard, T. Jessop, R. Lewis, B. Murray, P. Wender, Role of membrane potential and hydrogen bonding in the mechanism of translocation of guanidinium-rich peptides into cells, J. Am. Chem. Soc. 126 (2004) 9506–9507.
[16] N. Sakai, S. Matile, Anion-mediated transfer of polyarginine across liquid and bilayer membranes, J. Am. Chem. Soc. 125 (2003) 14348–14356.
[17] E. Goncalves, E. Kitas, J. Seelig, Binding of oligoarginine to membrane lipids and heparan sulfate: structural and thermodynamic characterization of a cell-penetrating peptide, Biochemistry 44 (2005) 2692–2702.
[18] E. Eiriksdottir, K. Konate, U. Langel, G. Divita, S. Deshayes, Secondary structure of cell-penetrating peptides controls membrane interaction and insertion, Biochim. Biophys. Acta 1798 (2010) 1119–1128.
[19] G. Lattig-Tunnemann, M. Prinz, D. Hoffmann, J. Behlke, C. Palm-Apergi, I. Morano, H. Herce, M. Cardoso, Backbone rigidity and static presentation of guanidinium groups increases cellular uptake of arginine-rich cell-penetrating peptides, Nat. Commun. 2 (2011) 453.
[20] M. Mammen, S.K. Choi, G.M. Whitesides, Polyvalent interactions in biological systems: implications for design and use of multivalent ligands and inhibitors, Angew. Chem. Int. Ed. 37 (1998) 2754–2794.
[21] L. Kiessling, J. Gestwicki, L. Strong, Synthetic multivalent ligands in the exploration of cell–surface interactions, Curr. Opin. Chem. Biol. 4 (2000) 696–703.
[22] M. Richter, A. Chakrabarti, I. Ruttekolk, B. Wiesner, M. Beyermann, R. Brock, J. Rademann, Multivalent design of apoptosis-inducing bid-BH3 peptide-oligosaccharides boosts the intracellular activity at identical overall peptide concentrations, Chem. Eur. J. 18 (2012) 16708–16715.
[23] D. Crothers, H. Metzger, The influence of polyvalency on the binding properties of antibodies, Immunochemistry 9 (1972) 341–357.
[24] S. Futaki, T. Suzuki, W. Ohashi, T. Yagami, S. Tanaka, K. Ueda, Y. Sugiura, Arginine-rich peptides. An abundant source of membrane-permeable peptides having potential as carriers for intracellular protein delivery, J. Biol. Chem. 276 (2001) 5836–5840.
[25] D.J. Mitchell, D.T. Kim, L. Steinman, C.G. Fathman, J.B. Rothbard, Polyarginine enters cells more efficiently than other polycationic homopolymers, J. Pept. Res. 56 (2000) 318–325.
[26] M. Sung, G.M. Poon, J. Gariepy, The importance of valency in enhancing the import and cell routing potential of protein transduction domain-containing molecules, Biochim. Biophys. Acta. 1758 (2006) 355–363.
[27] J.R. Johnson, H. Jiang, B.D. Smith, Zinc(II)-coordinated oligotyrosine: a new class of cell penetrating peptide, Bioconjug. Chem. 19 (2008) 1033–1039.
[28] G. Eggimann, S. Buschor, T. Darbre, J. Reymond, Convergent synthesis and cellular uptake of multivalent cell penetrating peptides derived from Tat, Antp, pVEC, TP10 and SAP, Org. Biomol. Chem. 50 (2013) 6717–6733.
[29] K.S. Kawamura, M. Sung, E. Bolewska-Pedyczak, J. Gariepy, Probing the impact of valency on the routing of arginine-rich peptides into eukaryotic cells, Biochemistry 45 (2006) 1116–1127.
[30] K. Koschek, M. Dathe, J. Rademann, Effects of charge and charge distribution on the cellular uptake of multivalent arginine-containing peptide-polymer conjugates, ChemBioChem. 14 (2013) 1982–1990.
[31] S.P. Liu, L. Zhou, R. Lakshminarayanan, R.W. Beuerman, Multivalent antimicrobial peptides as therapeutics: design principles and structural diversities, Int. J. Pept. Res. Ther. 16 (2010) 199–213.
[32] J. Imamura, Y. Suzuki, K. Gonda, C. Roy, H. Gatanaga, N. Ohuchi, H. Higuchi, Single particle tracking confirms that multivalent Tat protein transduction domain-induced heparan sulfate proteoglycan cross-linkage activates Rac1 for internalization, J. Biol. Chem. 286 (2011) 10581–10592.
[33] E. Larson, D. Doughman, D. Gregerson, W. Obritsch, A new, simple, nonradioactive, nontoxic in vitro assay to monitor corneal endothelial cell viability, Invest. Ophthalmol. Vis. Sci. 38 (1997) 1929–1933.
[34] S. Perrot, H. Dutertre-Catella, C. Martin, P. Rat, J. Warnet, Resazurin metabolism assay is a new sensitive alternative test in isolated pig cornea, Toxicol. Sci. 72 (2003) 122–129.
[35] M. Boyd, K. Paull, Some practical considerations and applications of the National Cancer Institute in vitro anticancer drug discovery screen, Drug Development Research 34 (1995) 91–109.
[36] O. Stoevesandt, K. Köhler, S. Wolf, T. André, W. Hummel, R. Brock, A network analysis of changes in molecular interactions in cellular signaling, Mol. Cell. Proteomics 6 (2007) 503–513.
[37] I. Ruttekolk, F. Duchardt, R. Fischer, K. Wiesmuller, J. Rademann, R. Brock, HPMA as a scaffold for the modular assembly of functional peptide polymers by native chemical ligation, Bioconjug. Chem. 19 (2008) 2081–2087.
[38] W. Verdurmen, R. Wallbrecher, S. Schmidt, J. Eilander, P. Bovee-Geurts, S. Fanghanel, J. Burck, P. Wadhwani, A. Ulrich, R. Brock, Cell surface clustering of heparan sulfate proteoglycans by amphipathic cell-penetrating peptides does not contribute to uptake, J. Control. Release 170 (2013) 83–91.
[39] G. Poon, J. Gariepy, Cell–surface proteoglycans as molecular portals for cationic peptide and polymer entry into cells, Biochem. Soc. Trans. 35 (2007) 788–793.
[40] S. Nakao, K. Komagoe, T. Inoue, T. Katsu, Comparative study of the membrane-permeabilizing activities of mastoparans and related histamine-releasing agents in bacteria, erythrocytes, and mast cells, Biochim. Biophys. Acta 1808 (2011) 490–497.
[41] T. Katsu, M. Kuroko, T. Morikawa, K. Sanchika, Y. Fujita, H. Yamamura, M. Uda, Mechanism of membrane damage induced by the amphipathic peptides gramicidin S and melittin, Biochim. Biophys. Acta 983 (1989) 135–141.
[42] T. Fujii, T. Sato, A. Tamura, M. Wakatsuki, Y. Kanaho, Shape changes of human erythrocytes induced by various amphipathic drugs acting on the membrane of the intact cells, Biochem. Pharmacol. 28 (1979) 613–620.
[43] F. Kamena, B. Monnanda, D. Makou, S. Capone, K. Patora-Komisarska, D. Seebach, On the mechanism of eukaryotic cell penetration by alpha- and beta-oligoarginines—targeting infected erythrocytes, Chem. Biodivers. 8 (2011) 1–12.
[44] D. Srinivasan, N. Muthukrishnan, G. Johnson, A. Erazo-Oliveras, J. Lim, E. Simanek, J. Pellois, Conjugation to the cell-penetrating peptide TAT potentiates the photodynamic effect of carboxytetramethylrhodamine, PLoS One 6 (2011) e17732.
[45] D. Delaroche, F.-X. Cantrelle, F. Subra, C. Van Heijenoort, E. Guittet, C.-Y. Jiao, L. Blanchoin, G. Chassaing, S. Lavielle, C. Auclair, S. Sagan, Cell-penetrating peptides with intracellular actin-remodeling activity in malignant fibroblasts, J. Biol. Chem. 285 (2010) 7712–7721.
[46] M. Yaffe, Phosphotyrosine-binding domains in signal transduction, Nat. Rev. Mol. Cell. Biol. 3 (2002) 177–186.
[47] C. Bollinger, V. Teichgraber, E. Gulbins, Ceramide-enriched membrane domains, Biochim. Biophys. Acta 1746 (2005) 284–294.
[48] A. Braiman, M. Barda-Saad, C.L. Sommers, L.E. Samelson, Recruitment and activation of PLCgamma1 in T cells: a new insight into old domains, EMBO. J. 25 (2006) 774–784.
[49] J.D. Dasgupta, C. Granja, B. Druker, L.L. Lin, E.J. Yunis, V. Relias, Phospholipase C-gamma 1 association with CD3 structure in T cells, J. Exp. Med. 175 (1992) 285–288.
[50] W. Zhang, B.J. Irvin, R.P. Trible, R.T. Abraham, L.E. Samelson, Functional analysis of LAT in TCR-mediated signaling pathways using a LAT-deficient Jurkat cell line, Int. Immunol. 11 (1999) 943–950.
[51] E. Aguado, M. Martínez-Florensa, P. Aparicio, Activation of T lymphocytes and the role of the adapter LAT, Transpl. Immunol. 17 (2006) 23–26.
[52] K. Köhler, A.C. Lellouch, S. Vollmer, O. Stoevesandt, A. Hoff, L. Peters, H. Rogl, B. Malissen, R. Brock, Chemical inhibitors when timing is critical: a pharmacological concept for the maturation of T cell contacts, ChemBioChem 6 (2005) 152–161.
[53] S. Futaki, I. Nakase, A. Tadokoro, T. Takeuchi, A.T. Jones, Arginine-rich peptides and their internalization mechanisms, Biochem. Soc. Trans. 35 (2007) 784–787.
[54] P.A. Wender, D.J. Mitchell, K. Pattabiraman, E.T. Pelkey, L. Steinman, J.B. Rothbard, The design, synthesis, and evaluation of molecules that enable or enhance cellular uptake: peptoid molecular transporters, Proc. Natl. Acad. Sci. U.S.A. 97 (2000) 13003–13008.
[55] B. Liu, Y. Huang, J. Winiarz, H. Chiang, H. Lee, Intracellular delivery of quantum dots mediated by a histidine- and arginine-rich HR9 cell-penetrating peptide through the direct membrane translocation mechanism, Biomaterials 32 (2011) 3520–3537.
[56] M. Lewin, N. Carlesso, C. Tung, X. Tang, D. Cory, D. Scadden, R. Weissleder, Tat peptide-derivatized magnetic nanoparticles allow in vivo tracking and recovery of progenitor cells, Nat. Biotechnol. 18 (2000) 410–414.
[57] K. Jan, S. Chien, Role of surface electric charge in red blood cell interactions, J. Gen. Physiol. 61 (1973) 638–654.
[58] B. Neu, R. Wenby, H.J. Meiselman, Effects of dextran molecular weight on red blood cell aggregation, Biophys. J. 95 (2008) 3059–3065.
[59] A. Pribush, D. Zilberman-Kravits, N. Meyerstein, The mechanism of the dextran-induced red blood cell aggregation, Eur. Biophys. J. 36 (2007) 85–94.
[60] M. Kosuge, T. Takeuchi, I. Nakase, A. Jones, S. Futaki, Cellular internalization and distribution of arginine-rich peptides as a function of extracellular peptide concentration, serum, and plasma membrane associated proteoglycans, Bioconjug. Chem. 19 (2008) 656–664.